MRS Communications (2018), 1 of 7

doi:10.1557/mrc.2018.83

MRS Communications

Research Letter

Tuning the photocurrent generations from photosystem I assembled in tailored biotic–abiotic interfaces

Hanieh Niroomand, Department of Chemical and Biomolecular Engineering; Sustainable Energy Education and Research Center (SEERC), University of Tennessee, Knoxville, TN 37996, USA*
Ravi Pamu, Department of Mechanical, Aerospace, and Biomedical Engineering; Nano-BioMaterials Laboratory for Energy, Energetics & Environment (nbml-E3), University of Tennessee, Knoxville, TN 37996, USA*
Dibyendu Mukherjee, Department of Mechanical, Aerospace, and Biomedical Engineering; Department of Chemical and Biomolecular Engineering; Nano-BioMaterials Laboratory for Energy, Energetics & Environment (nbml-E3); Sustainable Energy Education and Research Center (SEERC), University of Tennessee, Knoxville, TN 37996, USA
Bamin Khomami, Department of Chemical and Biomolecular Engineering; Department of Mechanical, Aerospace, and Biomedical Engineering; Sustainable Energy Education and Research Center (SEERC), University of Tennessee, Knoxville, TN 37996, USA

Address all correspondence to Bamin Khomami and Dibyendu Mukherjee at **bkhomami@utk.edu**, **dmukherj@utk.edu**

(Received 2 February 2018; accepted 16 April 2018)

Abstract

Rational design of bio-hybrid photovoltaic and/or optoelectronic devices requires systematic electrochemical characterizations of photosystem I (PSI), the photosynthetic membrane protein, assembled onto tailored biotic–abiotic interfaces. This work communicates our research findings on the role of PSI microenvironment alterations at organic/inorganic interfaces, via biomimetic lipid membrane confinements and plasmonic coupling with Ag nano-pyramid structures, in tuning the photoactivated charge separation and photocurrent generations from surface-assembled PSI. The observed photocurrent enhancements and the associated mechanistic insights from this study will facilitate the future design of tailored interfaces that can optimally tune the photoactivity and photostability of PSI in solid-state bioelectronics.

Introduction

Photosystem I (PSI), the photosynthetic membrane protein, goes through light-activated charge separation and unidirectional electron transfer with near-unity quantum efficiency. Based on the experimental photocurrent measurement of single PSI under specially designed conditions and theoretical photocurrent estimates due to its ultrafast excitation rates, it can reach up to few mA/cm^2 of photocurrent even from PSI monolayers.[1,2] Due to its great potential, robust structural, and photoelectrochemical (PEC) activities, PSI is an ideal biomaterial for bio-hybrid photovoltaic and/or optoelectronic devices. However, the first step toward the rational design of such devices demands systematic electrochemical characterizations of PSI assembly in tailored biotic–abiotic interfaces. In recent years, research has been directed toward immobilizing PSI onto conductive material [gold, titanium oxide, silicon, graphene, or gallium (III) arsenide, carbon nanotubes or other nanoparticles, and redox polymers].[1,3–6] Furthermore, PSI-based bio-hybrid photo sensors have been fabricated via wiring genetically mutated PSIs to electrodes, and photocurrent generations from these systems have been investigated.[4,6,7] Our past works have also demonstrated photocurrent generations from PSI monolayer immobilized on self-assembled monolayer (SAM)/Au substrates from colloidal suspensions using detergent-mediated chemistry and electric field-assisted assembly.[8–11] But, our efforts in depositing dense monolayers of PSI with preferential orientation of PSI and efficient photocurrent generation has only yielded limited success. To further enhance the efficiency of energy conversions in PSI/SAM-based assemblies, we have been targeting biomimetic confinements and plasmon-induced electric field enhancement strategies. Specifically, the ability to manipulate chromophore–chromophore interactions and energy transfer pathways within the PSI complex are being considered as the key critical steps in tuning the PSI photo activities. Hence, the role of microenvironment alterations and plasmon couplings in enhancing the efficiency, orientation, and lifetimes of light-activated PSI trimeric complexes deposited on various materials has been increasingly found prominence in our recent studies. We have investigated the effects of organic confinements via PSI incorporation into biomimetic lipid membrane scaffolds and plasmon-induced electric field variations on PSIs assembled

* These authors contributed equally to this work.

onto thiolated truncated Ag nano-pyramids with tuned plasmonic activities.

Firstly, to understand how microenvironment confinements regulate the inter-chromophore electronic coupling within the PSI complex, a high-density encapsulation of PSI in synthetic lipid bilayer membranes via detergent-mediated reconstitution will be considered.[12,13] To this end, the PSI-proteoliposomes were immobilized onto bio-hybrid electrodes and the PEC response of the system was subsequently characterized. In particular, detailed photocurrent investigations of specific alkanethiolate SAM ()/Au surfaces decorated with PSI encapsulated in DPhPG [1,2-diphytanoyl-*sn*-glycero-3-phospho-(1′-*rac*-glycerol)] liposomes will be presented here. Furthermore, photocurrent generations from PSI-proteoliposomes fabricated by using two non-ionic detergents Triton X-100 (TX-100) and *n*-dodecyl-*β*-D-maltoside (DDM) will also be reported.

The second part of the current study will examine the role of plasmon coupling on altering the PSI photocurrent generations by assembling PSI on Ag nanostructures whose plasmon peaks are specially adjusted to match the PSI absorption peaks. Localized surface plasmon resonance (LSPR) of metal nanoparticles are known to tune the optical properties of the adjacent biomolecules via nanoparticles-induced evanescent electric field at its resonant wavelength excitation.[14] This phenomenon has been utilized for enhancing the photocurrent in single chromophore dye molecule-based dye-sensitized solar cells[14–16] and multi-chromophore protein complexes.[17, 18] Except for an earlier theoretical work,[19] most previous studies on plasmon enhancement effects on PSI have largely focused on absorption and fluorescence effects[20–24] from PSIs immobilized on Ag and Au islands or Fischer's patterns of Ag and Au nano pyramids.[20–24] In the current work, we present the experimental verification of plasmon-enhanced photocurrent in PSI by immobilizing PSI on SAMs of OH-terminated thiols on Fischer's nano-patterns of Ag-nano pyramids (Ag-NPs) supported on conducting indium tin oxide (ITO) substrates.

Materials and methods

Aqueous buffer solutions of 200 mM sodium (Na) phosphate with pH = 7.0 was prepared using dibasic (Na_2HPO_4) and monobasic (NaH_2PO_4) Na phosphate with >99% assay (Fisher Scientific) in ultrapure de-ionized (DI) water (Millipore, Billerica, MA). NH_4OH and H_2O_2 for RCA wash were purchased from Fisher Chemicals. Non-ionic detergent, DDM and Triton X-100 (10% w/v aqueous solution) were purchased from Gold Biotechnology, MA and Anatrace, OH, respectively. Polycarbonate filters and DPhPG as lyophilized powders were purchased from Avanti Polar Lipids, Inc. Gold-coated silicon wafers (Au thickness ~100 nm) were purchased from Platypus Technologies.

Liposome preparation

A total of 4 mg/ml lipid suspensions were prepared in 200 mM Na phosphate (pH = 7.0) buffer, then freeze–thawed four times to form multilamellar liposomes and extruded using a NanoSizer Extrusion Kit (T&T Scientific) with 100 nm pore-sized filter at room temperature to form unilamellar vesicles. The 100 nm unilamellar vesicles were confirmed via dynamic light-scattering measurements. Further details can be found in the previous studies.[25]

Reconstitution of PSI

TX-100 and DDM were used for detergent-mediated protein reconstitutions. Each detergent was added to the preformed liposomes (4 mg/mL) and then followed by PSI reconstitution. Details regarding the PSI reconstitution using TX-100 can be found in our previous study.[12,13] For PSI reconstitution using DDM, the solution was equilibrated for 24 h, then mixed with the solubilized protein in 200 mM Na phosphate buffer (pH 7.0), and afterwards, the mixture was incubated for 30 min at room temperature under gentle agitation. The final [protein-to-lipid weight ratios (wPLR)] used for all our studies were 1.2. Consequently, DDM was removed by the addition of 30 mg Bio-Beads per 1 mg of DDM for 2 h at room temperature. Then, size-exclusion chromatography fractions were collected using a Sephacryl S-400 column attached to an AKTA purifier (GE) at a flow rate of 0.5 mL/min. The sample elution was monitored at 540 and 680 nm, thereby allowing the detection of both lipids and PSI.

PSI-proteoliposome immobilization on the alkanethiolate SAM/Au substrates

Details of alkanethiolate SAM/Au substrates preparations are provided in our previous work[12] where monolayers of C_4-COOH, C_4-OH, and C_6-OH were formed on Au substrates by immersing the substrates in 5 mM ethanolic solution of 4-mercaptobutyric acid (HS-C_3H_6-COOH, Sigma-Aldrich), 4-mercapto-1-butanol (HS-C_4H_8-OH, Sigma-Aldrich), and 6-mercapto-1-hexanol (HS-C_6H_{12}-OH, Sigma-Aldrich), respectively. Thereafter, 150 µl of protein–lipid suspensions were drop casted on the alkanethiolate SAM/Au substrates and incubated for 1 h at 45 °C. In turn, the samples were left at room temperature to cool for 1 h, thereby allowing the surface assembly of PSIs incorporated within the supported lipid bilayers (PSI-SLB). Subsequently, PSI-SLBs were washed several times at room temperature with Na phosphate buffer and DI water.

Preparation of Ag-NP Fischer patterns on ITO substrates

ITO-coated Na lime glass substrates (ITO thickness: 50–80 nm, NANOCS) were cleaned by 15 min of sonication in RCA (5 : 1 : 1 volume fractions of H_2O : 30% NH_4OH : 30% H_2O_2), followed by sonication in DI water for 15 min. Planar Ag substrates preparation was done by electron beam deposition (Model Mantis QUAD-EV-C) of Ag on cleaned ITO substrates under high vacuum ($\sim 1 \times 10^{-8}$ Torr) at room temperature. Ag-NPs were prepared using 500 nm size polystyrene latex beads in 2.5 wt% dispersion (Alfa Aesar-42714) diluted with ethanol (1 : 10 volume fractions). The diluted beads solution was then added drop by drop on to the base of the Petri dish

glass partially filled with DI water. By pushing each drop close to the glass–water–air triple interface of Petri dish, the surface tension gradient forces the beads to migrate to the surface of water in the dish. This process is repeated until the beads cover the entire water surface with high packing density. The Petri dish was then filled with water. The hexagonally packed monolayer of the beads with lowest defects was detected with its interference pattern on the water surface and lifted onto a clean ITO substrate. Then, electron beam deposition was used to deposit 81 ± 4 nm-thick Ag layer on ITO substrates. Subsequently, the substrate was sonicated in ethanol for 1 min to remove the polymer bead mask, leaving the Ag-NP Fischer patterns on ITO.

Immobilization of PSI on various SAM substrates

SAM deposition on different substrates was done by immersing ITO, planar Ag, and Ag-NP/ITO substrates in 5 mM 6-mercapto-1-hexanol (Sigma-Aldrich) solution in ethanol for 7 days at room temperature under N_2 environment. Afterward, SAM/ITO, SAM/planar Ag, and SAM/Ag-NP/ITO substrates were cleaned by immersing in isopropanol. Sonication is avoided to prevent dislodging of the Ag-NPs from the ITO surface. The cyanobacterial PSI complexes[26] were immobilized on SAM-treated substrates by immersing the substrate in PSI solution (0.013 µM of PSI in 200 mM Na phosphate buffer (pH = 7) with 0.02% w/v DDM) for 24 h at room temperature in dark. Finally, the PSI/SAM/ITO, PSI/SAM/Ag, and PSI/SAM/Ag-NP/ITO substrates were rinsed with DI water and dried in an N_2 stream.

Atomic force microscopy

Gold-coated silicon wafers (Au thickness ~100 nm) were immersed in isopropanol and DI water for 10 min, and dried under N_2. PSI-proteoliposomes were immobilized on the gold wafers by placing 200 µl of PSI-proteoliposome suspension after size exclusion chromatography onto Au wafers. The wafers were then allowed to dry for 1 h at 158 °F and 1 h at room temperature, and then rinsed in DI water and dried under N_2. Atomic force microscopy (AFM) images were taken in the non-contact (tapping) mode using an NT-MDT microscope and silicon cantilevers (0.35–6.1 N/m, NT-MDT; Model: NSG03).

Scanning electron microscopy

Scanning electron microscopy (SEM) images of the Ag-NP/ITO electrode surface have been taken using a Zeiss Merlin SEM at 3 kV. HR2000 + ES spectrometer (Ocean Optics) was used to obtain the plasmonic resonance peaks from the optical transmission spectrum of Ag-NP/ITO electrodes.

Electrochemical and PEC characterization

A custom-built three-electrode cells electrochemistry setup with a Bio-Logic potentiostat (Model: SP-300) was used for photocurrent measurements. In this setup, Au, ITO, PlanarAg, and Ag-NP/ITO substrates were used as the working electrodes and a Pt counter electrode and an Ag/AgCl (sat. NaCl) reference electrode were used. In all experiments, 1 mM aqueous methyl viologen (MV; soluble electron scavenger) and 100 mM KCl (supporting electrolyte) were used. The four collimated light-emitting diodes (LEDs) with the nominal wavelengths of 395, 420, 470, and 660 nm (ThorLabs; Model: M395L4, M420L3, M470L3, M660L4) were operated with a power density of 36 mW/cm^2 reaching the working area when the solution in the cell was absent. Photocurrent measurements of PSI-proteoliposomes were conducted using the 660 nm LED source. All photocurrent measurements were conducted at open-circuit voltage with 2 min on/off light cycles and repeated for at least six cycles.

Results

High-density encapsulation of PSI in synthetic lipid bilayer membranes was carried out by incorporating PSI solubilized with prototypical non-ionic detergents, either Triton X-100 (TX-100) or DDM. The liposomes were destabilized with TX-100 at a detergent concentration of $C_{Trit} = 12.0$ mM and with DDM at a detergent concentration of $C_{DDM} = 9.6$ mM. After PSI insertion, the excess detergent was removed using polystyrene beads (see "Materials and methods" section). In turn, size-exclusion chromatography fractions were collected. The final wPLR is 1.2 throughout this study. Finally, PSI-proteoliposome suspensions were drop casted onto –COOH and –OH terminated thiol SAM/Au substrates and assembled into the PSI-LB (PSIs incorporated within lipid bilayers) electrodes.

PEC characterizations of PSIs incorporated within biomimetic lipid membrane scaffolds

Chronoamperometry measurements were performed on PSI-LB electrodes under light and dark conditions with the addition of MV as the electron scavenger under aerobic conditions. The maximum photocurrent density obtained from PSI-LB electrodes on various SAM substrates with different terminal chemistries and PSI-proteoliposomes reconstituted with different detergents (DDM and TX-100) are given in Fig. 1 and Table I.

Surface topography AFM images of SAM/Au substrates treated with PSI-proteoliposomes that are reconstituted using TX-100 and DDM are shown in Fig. 2. These images reveal semi-uniform monolayer of PSIs within the TX-100-mediated PSI-LB, as well as the presence of some intact liposomes, which have not fully collapsed on the SAM [Figs. 2(a)–2(c)]. The inset indicates approximate width of 100–150 nm and average heights of 20–25 nm for intact liposomes. Typical average protein diameters of ~25 nm and average heights of ~3 nm (on top of 5 nm lipid bilayer) are obtained from the cross-sectional analysis of PSI-proteoliposomes deposition on all SAM/Au surfaces (Supplementary Information, Figs. S1 and S2). These values correspond very well with the typical PSI diameters of ~25–30 nm and heights of ~9 nm.

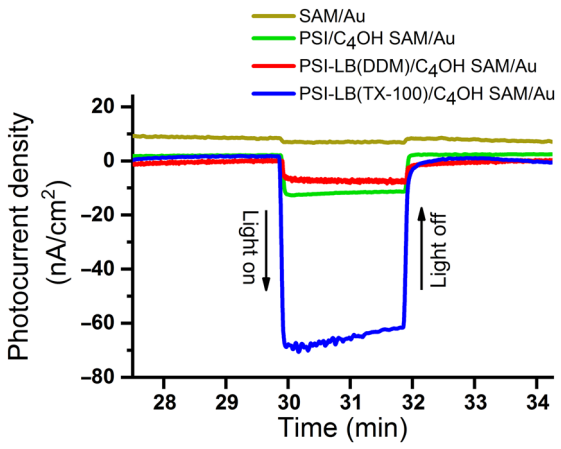

Figure 1. Chronoamperometry data of photocurrents from light on–off experiments on PSI/C_4OH SAM/Au, PSI-LB/C_4OH SAM/Au prepared using DDM as the detergent, and PSI-LB/C_4OH SAM/Au prepared using TX-100 substrates at OCV versus Ag/AgCl under illumination (λ = 660 nm) under aerobic conditions. The photocurrent of SAM-treated Au substrate without the addition of PSI (gold line) is moved up for ease of visualization.

However, in the case of DDM-mediated PSI-LB, sparse layers of PSIs within the LB were observed [Figs. 2(d)–2(f)]. These observations indicate that DDM is not the ideal choice of detergents for successful PSI-proteoliposome formation, while TX-100 turns out to be a promising detergent for achieving PSI-LBs. It should be pointed out that photocurrents generated from TX-100-mediated PSI-LB electrodes indicate stable photocurrents even after 30 min. In recent years, growing evidence suggests that there is a direct link between the absence of lipid membranes and rapid deactivation of the photosynthetic proteins, photosystem II, and PSI integrated into electrodes.[27–29] Measurements from the organic microenvironment confinement of PSI in our system indicate stable photocurrents, which confirm that synthetic lipid membranes, when used as protein scaffolds, can enhance the stability of such systems. Achieving significantly high photocurrent (in the range of mA/cm^2) from PSI monolayers requires high packing density, systematic confinement, and correct orientation of PSIs on the substrate. We have successfully performed a dense and uniform monolayer of PSI on the SAM-modified substrates; however, the photocurrent obtained from this substrate is 14.5 μA/cm^2 (refer to Fig. 1) due to the lack of tailored orientation and confinement. Sparse layers of PSIs within the LB showed enhanced photocurrents up to 63 μA/cm^2 (refer to Fig. 1) and improved stability. Although, the intact liposomes act as an insulator and decrease the photocurrent generated from these systems, photocurrent densities were normalized per number of protein to eliminate the contribution of the intact liposomes.

Table I. Photocurrents densities generated from PSI-LB electrodes treated with different terminal chemistries.

	Photocurrent densities (nA/cm^2)		
Detergent type	PSI-LB/C_4COOH SAM/Au	PSI-LB/C_4OH SAM/Au	PSI-LB/C_6OH SAM/Au
TX-100	40.5 ± 1.6	63 ± 2.1	60 ± 1.1
DDM	4.2 ± 0.2	7.8 ± 0.3	8 ± 0.3

PEC characterizations of PSIs assembled on truncated plasmonic Ag nano-pyramids

As shown in Fig. 3(a), the Fischer patterns of Ag-NP on ITO were adjusted to match the PSI absorption at 450 and 680 nm regions for optimal plasmonic coupling. The peak position of Ag-NP/ITO substrates were observed to be largely dependent on the percentage of defects in the substrate, which arose from the defects in the hexagonal packing of monolayer polystyrene beads as a mask in preparing the substrate. The Ag-NP height or Ag deposition thickness of ~81 ± 4 nm with the 500 nm polystyrene beads mask was observed to be the ideal parameters for achieving the aforementioned plasmonic peak positions. The average Ag-NPs base area was 14,024.76 nm^2. Since the beads mask was arranged in a hexagonal pattern, the fraction of apparent ITO area [considering Ag-NP as two-dimensional (2D) Δ plate] was 0.903, which is close to the hexagonal packing fraction of 0.907. The self-assembly methods developed previously[9,11] were used to prepare PSI immobilization on SAM-coated Ag-NP/ITO to make the PSI/SAM/Ag-NP/ITO substrate. This substrate acted as the working electrode in our standard three electrodes electrochemical cell set-up. It was tested for photocurrents at four excitation wavelengths of interest: 395, 420, 470, and 660 nm. To estimate the photocurrent enhancement factors, the photocurrents measured from the prepared electrodes of PSI/SAM/ITO and PSI/SAM/Ag were compared with the photocurrent recorded from smooth continuous bare ITO and Ag substrates that were coated with PSI in a similar fashion. Background photocurrents of SAM-coated electrodes (SAM/Ag-NP/ITO, SAM/Ag, SAM/ITO) being significant, the effective photocurrents obtained from PSI on the three specific substrates of Ag-NP/ITO, flat Ag, and flat ITO were evaluated by subtracting the respective background photocurrents from the values for the PSI-coated electrodes.

The effective photocurrents from PSI on the aforementioned three substrate electrodes at the four excitation wavelengths are shown in Fig. 3(b). A distinctive trend is observed for the effective PSI-driven photocurrents from the Ag-NP/ITO electrodes that can be readily ascribed to the plasmon-coupled photocurrent enhancements. There is an apparent enhancement in the PSI photocurrents measured from the Ag-NP/ITO electrode for 420, 470, and 660 nm excitations as compared with the respective values recorded for the flat Ag electrodes. Here, the effective photocurrents were normalized with the nominal 2D surface areas of the electrodes. Due to the low roughness of the Ag and ITO substrates, it is assumed that the nominal surface area is same as the effective surface area for Ag and ITO

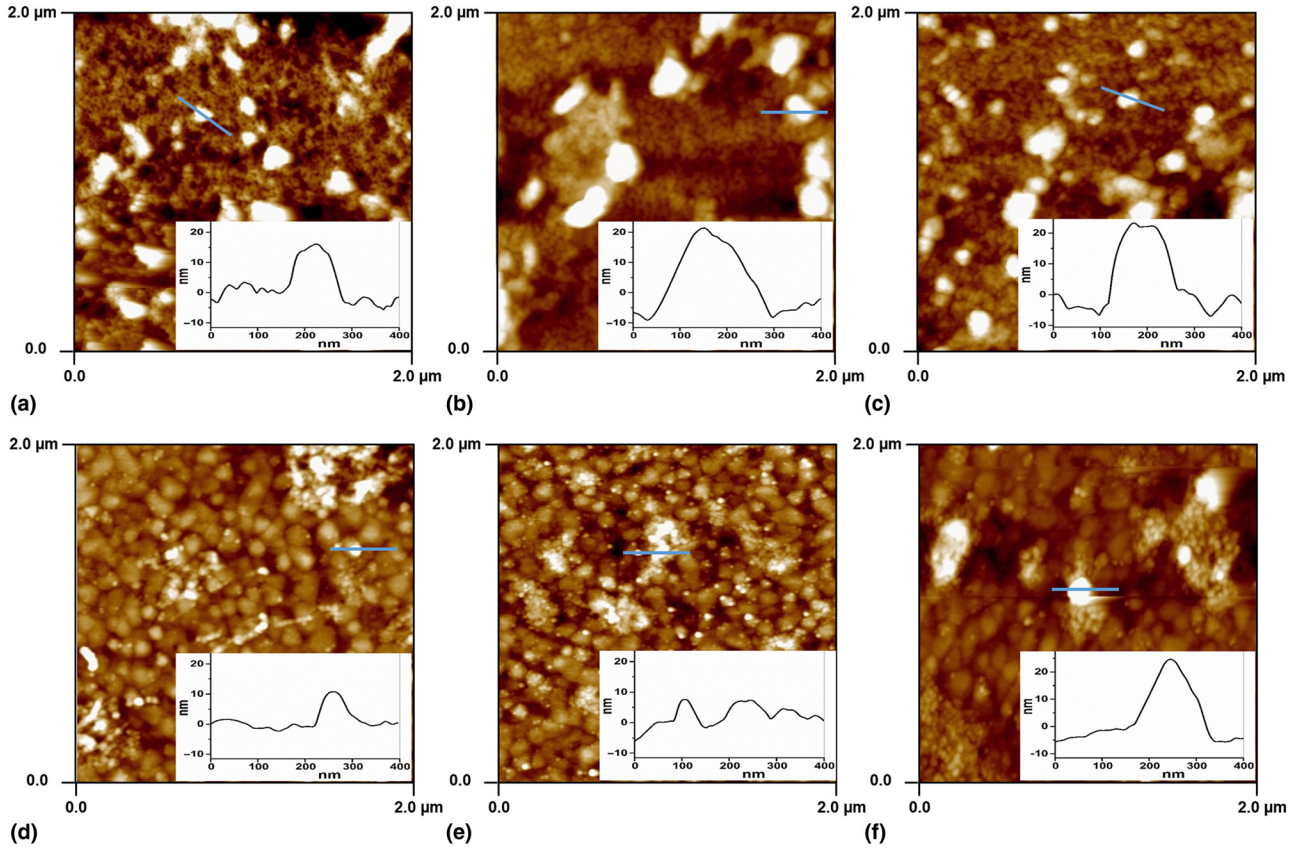

Figure 2. AFM images showing the surface topographies of SAM/Au substrates treated with PSI-proteoliposomes reconstituted with (a–c) TX-100 and (d–f) DDM. Substrates were treated with different terminal chemistries (a, d) C_4COOH; (b, e) C_4OH; and (c, f) C_6OH (insets: height profiles of marked lines in each panel).

electrodes. The PSI trimer densities (number of PSI trimers per unit area) on Ag and ITO reference electrodes were estimated from the AFM images of PSI/SAM/Ag and PSI/SAM/ITO. Based on this information, the effective photocurrent (nA) per unit PSI trimer on the Ag and ITO ($P_{Ag}$and P_{ITO}) substrates was evaluated from the ratio of effective photocurrent density

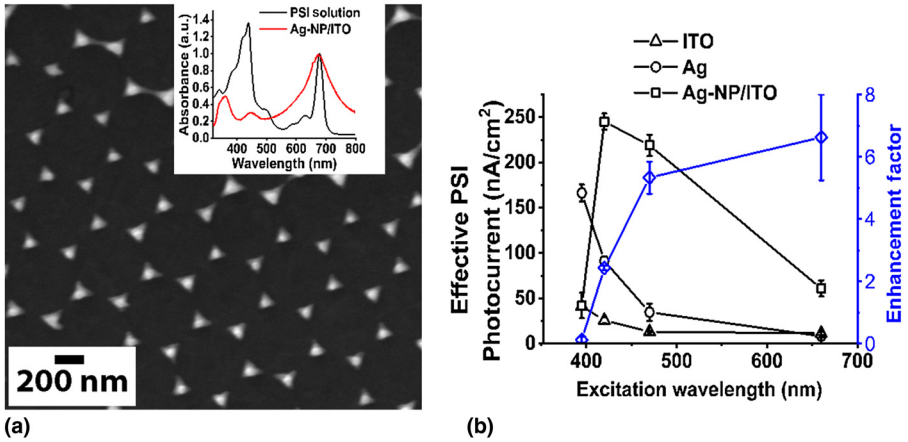

Figure 3. (a) SEM image of Ag nano-pyramids on ITO (Ag-NP/ITO substrate). Inset: the absorptions spectrum of PSI solution (black) and Ag-NP/ITO substrate. (b) Effective absolute value of photocurrents of PSI/SAM and SAM-treated ITO, planar Ag, Ag-NP/ITO electrodes with nominal surface area normalization. The blue trend with right side *y*-axis represents the final plasmon-induced photocurrent enhancement factors estimated based on the ratio of effective photocurrent per PSI on Ag-NPs to the non-plasmonic Ag.

(nA/cm^2) to the PSI trimer density. This effective photocurrent per PSI on flat Ag (P_{Ag}) substrate was used as a reference for establishing the plasmon-induced photocurrent enhancement factors.

In case of Ag-NP/ITO, the additional surface areas created by the nano-pyramid structures is ~0.323 times the nominal 2D-projected surface area of the substrate. This factor is established from the careful analysis of the AFM and SEM images taken for the Ag-NP/ITO substrate. Since the PSI trimers are distributed on both the Ag-NP and the ITO areas of the AgNP/ITO substrate, the effective photocurrent obviously bears contributions from PSIs located on nano-pyramid and ITO areas. Here, one can assume that the PSIs sitting on ITO parts would experience negligible plasmonic effects from the Ag NPs since the PSI/SAM layer is ~10 nm thick and plasmon-induced electric fields are typically highly localized that decay rapidly from the metal surfaces.[16] Furthermore, the effective photocurrents from PSI on flat ITO substrates are minimal [see Fig. 3(b)]. Thus, one can easily justify the separation of the effective PSI photocurrents from the Ag-NP/ITO substrate into two parts: (1) effective photocurrents from PSI on the Ag-NPs (under LSPR-induced electric field) and (2) effective photocurrents from PSI on the ITO areas can be easily justifiable.

The final plasmon-induced photocurrent enhancement factors were determined by the ratio of P_{AgNP}/P_{Ag} and are depicted in Fig. 3(b). The mean value for the photocurrent enhancement factors significantly increases to ~5.8 and ~6.5 at the excitation wavelengths of 470 and 660 nm, respectively.

Discussion

Chronoamperometry measurements of PSI-LB electrodes at the excitation wavelengths of 660 nm (see Fig. 4) reveal that photocurrents generated from TX-100-mediated PSI-LB electrodes are seven to ten times higher than that from DDM-mediated PSI-LB electrodes with equivalent PSI concentrations. Additionally, these measurements revealed that photocurrents generated from lipid-confined PSI are four to five times higher than that from the dense monolayer of individual PSI on SAM substrates with equivalent PSI concentrations (0.035 μM PSI trimer). Furthermore, chronoamperometry measurements of PSI deposition on various SAM-treated substrates at the excitation wavelengths of 660 nm reveal that photocurrents obtained from PSI/SAM/Ag-NP/ITO electrodes are ~3 times higher than that from SAM/Ag-NP/ITO electrodes and ~9 times higher than that from PSI/SAM/ITO electrodes.

Summary and conclusion

In this communication, we have presented the highlights from our recent investigations into the role of biotic (lipid membrane) and abiotic (plasmonic metal nanostructures) microenvironment alterations in tuning the highly efficient photoactivated charge separation and photocurrent generations of PSI assembled on electrodes. Specifically, we have shown that confinements through biomimetic lipid membrane scaffolds alter PSI photoactivity and enhance its stability. Also, direct visualizations using AFM imaging and photocurrent measurements clearly show that TX-100-mediated PSI-LBs tend to be more robust and superior as compared with the DDM-mediated PSI-LBs both in terms of the number of PSIs encapsulated per LB and evidently, the photocurrent enhancements. Finally, the plasmon-enhanced photocurrent effects in PSI assemblies was investigated by immobilizing PSIs on Fischer-patterned Ag-NPs whose resonant plasmonic peaks were tuned to match the PSI absorption peaks at λ ~450 and ~680 nm wavelengths. In turn, such arrangements result in boosting the photocurrent enhancement factors.

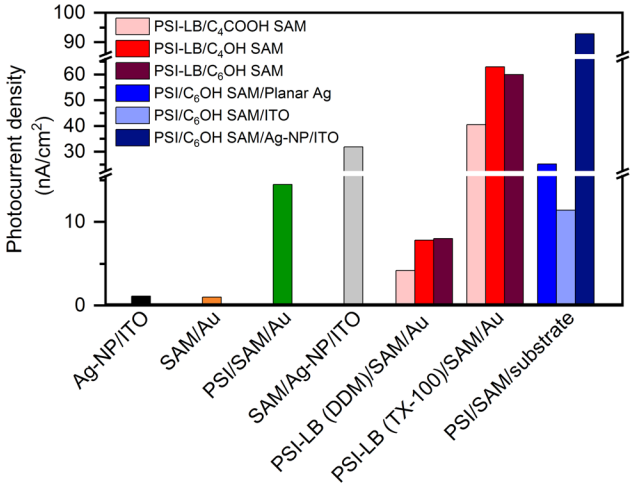

Figure 4. Comparisons of the maximum photocurrent densities obtained from PSI deposition on various types of SAM-treated substrates. Representative results compared here for PSI-LB/SAM/Au substrates made from PSI-proteoliposomes reconstituted with 12 mM TX-100 or 9.6 mM DDM.

Supplementary material

The supplementary material for this article can be found at https://doi.org/10.1557/mrc.2018.83

Acknowledgments

The authors would like to acknowledge the University of Tennessee Bioanalytical Resources Facility for instrument use and Dr Edward Wright for scientific and technical assistance. The authors thank Dr Graham J. Taylor for helping them preparing the liposome suspension. This work was funded in part by the Sustainable Energy Education and Research Center (SEERC) at the University of Tennessee, Knoxville and the Gibson Family Foundation.

References

1. D. Gerster, J. Reichert, H. Bi, J.V. Barth, S.M. Kaniber, A.W. Holleitner, I. Visoly-Fisher, S. Sergani, and I. Carmeli: Photocurrent of a single photosynthetic protein. *Nat. Nanotechnol.* **7**, 673 (2012).
2. K. Brettel and W. Leibl: Electron transfer in photosystem I. *Biochim. Biophys. Acta Bioenerg.* **1507**, 100 (2001).

3. I. Carmeli, M. Mangold, L. Frolov, B. Zebli, C. Carmeli, S. Richter, and A. W. Holleitner: A photosynthetic reaction center covalently bound to carbon nanotubes. *Adv. Mater.* **19**, 3901 (2007).
4. L. Frolov, Y. Rosenwaks, C. Carmeli, and I. Carmeli: Fabrication of a photoelectronic device by direct chemical binding of the photosynthetic reaction center protein to metal surfaces. *Adv. Mater.* **17**, 2434 (2005).
5. G. LeBlanc, K.M. Winter, W.B. Crosby, G.K. Jennings, and D.E. Cliffel: Integration of photosystem I with graphene oxide for photocurrent enhancement. *Adv. Energy Mater.* **4**, 5 (2014).
6. N. Terasaki, N. Yamamoto, T. Hiraga, Y. Yamanoi, T. Yonezawa, H. Nishihara, T. Ohmori, M. Sakai, M. Fujii, A. Tohri, M. Iwai, Y. Inoue, S. Yoneyama, M. Minakata, and I. Enami: Plugging a molecular wire into photosystem I: reconstitution of the photoelectric conversion system on a gold electrode. *Angew. Chem. Int. Ed.* **48**, 1585 (2009).
7. N. Terasaki, N. Yamamoto, M. Hattori, N. Tanigaki, T. Hiraga, K. Ito, M. Konno, M. Iwai, Y. Inoue, S. Uno, and K. Nakazato: Photosensor based on an FET utilizing a biocomponent of photosystem I for use in imaging devices. *Langmuir* **25**, 11969 (2009).
8. T. Bennett, H. Niroomand, R. Pamu, I. Ivanov, D. Mukherjee, and B. Khomami: Elucidating the role of methyl viologen as a scavenger of photoactivated electrons from photosystem I under aerobic and anaerobic conditions. *Phys. Chem. Chem. Phys.* **18**, 8512 (2016).
9. D. Mukherjee, M. May, and B. Khomami: Detergent-protein interactions in aqueous buffer suspensions of photosystem I (PS I). *J. Colloid Interface Sci.* **358**, 477 (2011).
10. D. Mukherjee, M. May, M. Vaughn, B.D. Bruce, and B. Khomami: Controlling the morphology of photosystem I assembly on thiol-activated Au substrates. *Langmuir* **26**, 16048 (2010).
11. D. Mukherjee, M. Vaughn, B. Khomami, and B.D. Bruce: Modulation of cyanobacterial photosystem I deposition properties on alkanethiolate Au substrate by various experimental conditions. *Colloids Surf. B* **88**, 181 (2011).
12. H. Niroomand, D. Mukherjee, and B. Khomami: Tuning the photoexcitation response of cyanobacterial photosystem I via reconstitution into proteoliposomes. *Sci. Rep.* **7**, 2492 (2017).
13. H. Niroomand, G.A. Venkatesan, S.A. Sarles, D. Mukherjee, and B. Khomami: Lipid-detergent phase transitions during detergent-mediated liposome solubilization. *J. Membr. Biol.* **249**, 523 (2016).
14. T. Akiyama, M. Nakada, N. Terasaki, and S. Yamada: Photocurrent enhancement in a porphyrin-gold nanoparticle nanostructure assisted by localized plasmon excitation. *Chem. Commun.* **4**, 395 (2006).
15. S.-J. Lin, K.-C. Lee, J.-L. Wu, and J.-Y. Wu: Plasmon-enhanced photocurrent in dye-sensitized solar cells. *Sol. Energy* **86**, 2600 (2012).
16. S.D. Standridge, G.C. Schatz, and J.T. Hupp: Distance dependence of plasmon-enhanced photocurrent in dye-sensitized solar cells. *J. Am. Chem. Soc.* **131**, 8407 (2009).
17. V.M. Friebe, J.D. Delgado, D.J. Swainsbury, J.M. Gruber, A. Chanaewa, R. van Grondelle, E. von Hauff, D. Millo, M.R. Jones, and R.N. Frese: Plasmon-enhanced photocurrent of photosynthetic pigment proteins on nanoporous silver. *Adv. Funct. Mater.* **26**, 285 (2016).
18. C.-W. Yen, L.-K. Chu, and M.A. El-Sayed: Plasmonic field enhancement of the bacteriorhodopsin photocurrent during its proton pump photocycle. *J. Am. Chem. Soc.* **132**, 7250 (2010).
19. A.O. Govorov and I. Carmeli: Hybrid structures composed of photosynthetic system and metal nanoparticles: plasmon enhancement effect. *Nano Lett.* **7**, 620 (2007).
20. J.B. Nieder, R. Bittl, and M. Brecht: Fluorescence studies into the effect of plasmonic interactions on protein function. *Angew. Chem. Int. Ed.* **49**, 10217 (2010).
21. N. Czechowski, H. Lokstein, D. Kowalska, K. Ashraf, R. Cogdell, and S. Mackowski: Large plasmonic fluorescence enhancement of cyanobacterial photosystem I coupled to silver island films. *Appl. Phys. Lett.* **105**, 043701 (2014).
22. M. Brecht, M. Hussels, J.B. Nieder, H. Fang, and C. Elsässer: Plasmonic interactions of photosystem I with Fischer patterns made of gold and silver. *Chem. Phys.* **406**, 15 (2012).
23. I. Kim, S.L. Bender, J. Hranisavljevic, L.M. Utschig, L. Huang, G. P. Wiederrecht, and D.M. Tiede: Metal nanoparticle plasmon-enhanced light-harvesting in a photosystem I thin film. *Nano Lett.* **11**, 3091 (2011).
24. I. Ashraf, A. Konrad, H. Lokstein, S. Skandary, M. Metzger, J.M. Djouda, T. Maurer, P.M. Adam, A.J. Meixner, and M. Brecht: Temperature dependence of metal-enhanced fluorescence of photosystem I from thermosynechococcus elongates. *Nanoscale* **9**, 4196 (2017).
25. D. Lichtenberg and Y. Barenholz: *Liposomes: Preparation, Characterization, and Preservation, Methods of Biochemical Analysis* (John Wiley & Sons, Inc., New York, 1988), pp. 337, 462.
26. R.K. Le, M. Raeeszadeh-Sarmazdeh, E.T. Boder, and P.D. Frymier: Sortase-mediated ligation of PsaE-modified photosystem I from *Synechocystis* sp. PCC 6803 to a conductive surface for enhanced photocurrent production on a gold electrode. *Langmuir* **31**, 1180 (2015).
27. M.M. Nowaczyk and N. Plumere: Photosynthesis: short circuit at the chlorophyll. *Nat. Chem. Biol.* **12**, 990 (2016).
28. J.Z. Zhang, K.P. Sokol, N. Paul, E. Romero, R. van Grondelle, and E. Reisner: Competing charge transfer pathways at the photosystem II-electrode interface. *Nat. Chem. Biol.* **12**, 1046 (2016).
29. K.P. Sokol, D. Mersch, V. Hartmann, J.Z. Zhang, M.M. Nowaczyk, M. Rogner, A. Ruff, W. Schuhmann, N. Plumere, and E. Reisner: Rational wiring of photosystem II to hierarchical indium tin oxide electrodes using redox polymers. *Energy Environ. Sci.* **9**, 3698 (2016).